

Takashi Kimura

## Contents

Introduction .....	1577
Generation, Diffusion, and Detection of Pure Spin Current .....	1578
Advantage of Lateral Configuration .....	1581
Spin Absorption Effect .....	1585
Influence of an Additional Contact .....	1585
Transverse Spin Current Absorption into Ferromagnetic Metal .....	1586
Reabsorption Effect of Spin Current .....	1588
Magnetization Switching Due to Injection of Pure Spin Current .....	1591
Conclusion and Outlook .....	1594
References .....	1594

---

## Abstract

The transport properties of the diffusive pure spin current induced in the metallic nanostructures are discussed. The author introduces the methods for the efficient generation, manipulation, and detection of the pure spin current in laterally configured ferromagnetic/nonmagnetic metal hybrid structures. The experimental demonstration of the magnetization switching using the pure spin current is also introduced.

---

## Introduction

Ferromagnetic metal (FM)/nonmagnetic metal (NM) hybrid nanostructures show intriguing electrical transports in association with the spin accumulation and the spin momentum transfer [1–3]. In such spin-dependent transports, spin current, a

---

T. Kimura (✉)

Department of Physics, Inamori Frontier Research Center, Kyushu University, Fukuoka, Japan  
e-mail: [t-kimu@phys.kyushu-u.ac.jp](mailto:t-kimu@phys.kyushu-u.ac.jp)

flow of the spin angular momentum, is the key ingredient [4]. Therefore, the study on the transport properties of the spin current is essential for deeply understanding the fundamental physics of the spin-dependent transports as well as for further developing the spintronic devices. In order to investigate the spin current property, till to date, most experiments by other groups have been carried out in a vertical structure called the current-perpendicular-to-plane (CPP) configuration [5, 6]. It is, however, difficult to fabricate multiterminal devices with vertical structures, so one can obtain only limited information about the series resistance of the magnetic multilayers. On the other hand, laterally configured FM/NM hybrid nanostructures have great advantage for developing the multiterminal spintronic devices because of their flexible configuration [7, 8]. Especially, a pure spin current created by a nonlocal spin injection is a powerful tool for detecting the electric signals purely related to the spin transports [9–12] as in this case, the charge-current-induced spurious signals such as anisotropic magnetoresistance and the anomalous Hall effect can be removed. In this chapter, the author describes the transport property of the diffusive spin current in lateral nanostructures and introduces unique techniques for the efficient manipulation of spin current.

---

## Generation, Diffusion, and Detection of Pure Spin Current

A laterally configured ferromagnetic (F)/nonmagnetic (N) hybrid structure combined with a nonlocal spin injection allows to create a flow of spins without a flow of electrical charges, i.e., pure spin current [7–11, 13, 14]. Figure 1 shows a schematic illustration of the nonlocal spin injection. A bias voltage for the spin injection is applied between the ferromagnet and left-hand side nonmagnet. In this case, the spin-polarized electrons are injected from the ferromagnet and are extracted from the left-hand side of the nonmagnet. This results in the accumulation of the nonequilibrium spins in the vicinity of the F/N junctions. Since the electrochemical potential in the left-hand side is lower than that underneath the F/N junction, the electron flows by the electric field. In the right-hand side, although there is no electric field, the diffusion process from the nonequilibrium into the equilibrium state induces the motion of the electrons. Since the excess up-spin electrons exist underneath the F/N junction, the up-spin electrons diffuse into the right-hand side. On the other hand, the deficiency of the down-spin electrons induces the incoming flow of the down-spin electrons opposite to the motion of the up-spin electron. Thus, a pure spin current, which carries the spin angular momentum without electrical charges, can be induced by the nonlocal spin injection.

The induced pure spin current can be detected by using another FM voltage probe. Here, a four-terminal structure, in which two ferromagnetic electrodes are separately connected to a NM strip, is considered, as shown in Fig. 2a. When the pure spin current is injected into the FM, a shift in the electrostatic potential of the FM is induced because of the spin-dependent conductivity. The sign of the potential shift depends on the relative angle between the spin direction of the injecting spin

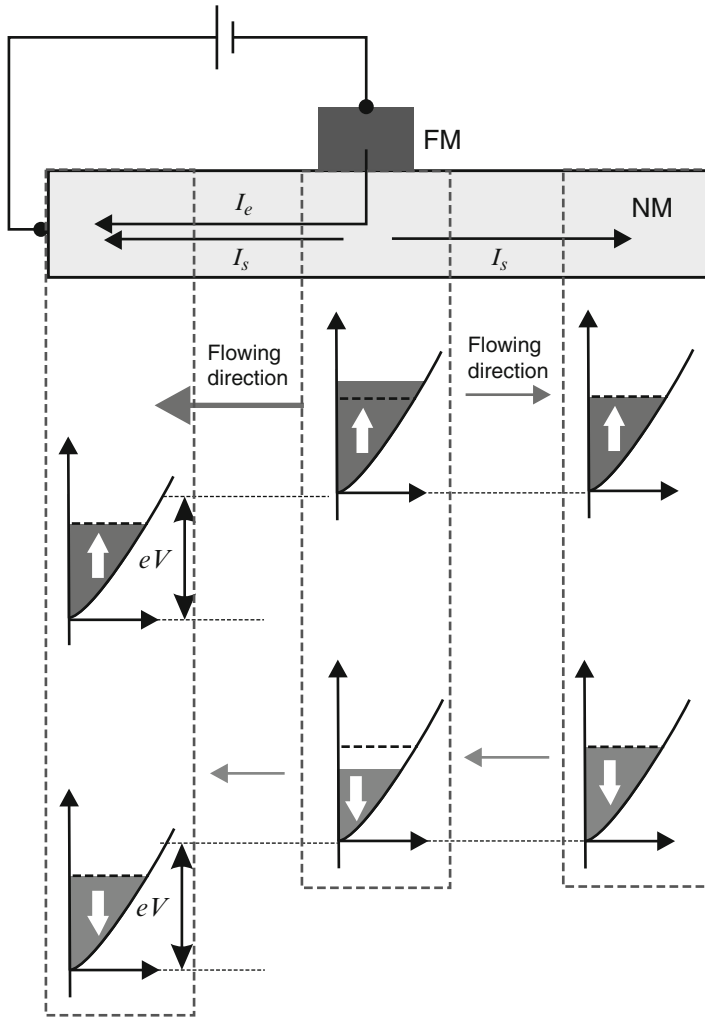


**Fig. 1** Schematic illustration of the nonlocal spin injection together with the density of states for the up-spin and down-spin electrons in nonmagnetic metal for left-hand, center, and right-hand sides

current and the magnetization direction. When the direction of the injecting spin is parallel to the majority (minority) spin for the spin detector, the electrostatic potential of the spin detector shifts positively (negatively). Therefore, when the voltage between the FM and the right-hand side of the NM is measured with sweeping the magnetic field, a clear voltage change is observed. The voltage normalized by the injecting current is known as the spin signal [7–11, 13, 14].

Figure 2b shows a representative nonlocal signal as a function of the external magnetic field observed in the Py/Cu lateral nonlocal spin valve measured at 77 K. Here, the center-center distance between the Py injector and detector is 800 nm.

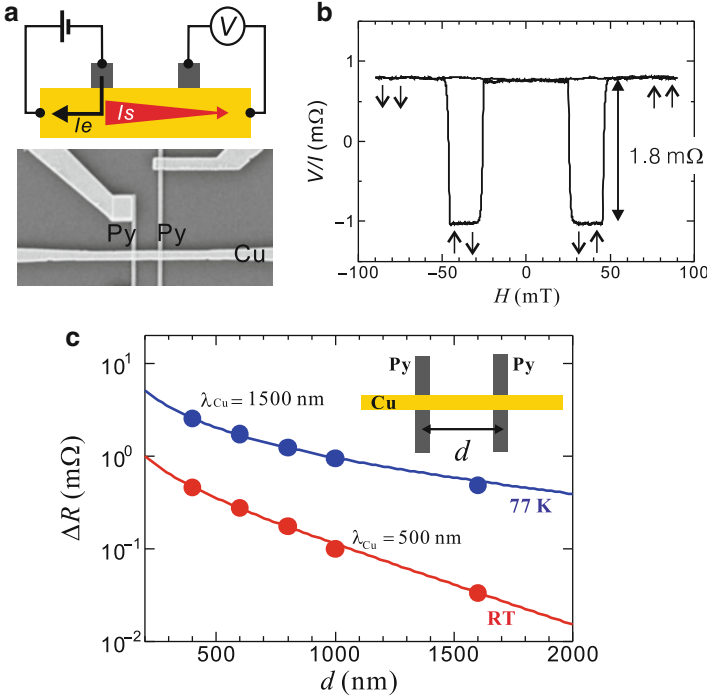


**Fig. 2** (a) Schematic illustration of the nonlocal spin injection and detection together with a SEM image of a typical lateral spin valve consisting of Py and Cu wires. (b) Typical nonlocal spin-valve signal for the Py/Cu device with a distance of 800 nm. (c) Position dependence of the nonlocal spin-valve signals at RT and 77 K

The field dependence of the nonlocal spin signal exhibits a clear spin-valve effect corresponding to parallel (high) and antiparallel (low) states. By changing the distance between the injector and detector, one can experimentally estimate the spin diffusion length of the Cu wire. As can be seen in Fig. 2c, the spin signal monotonically decreases with increasing the distance  $d$  both at RT and 77 K because of the spin relaxation phenomenon.

From the one-dimensional spin diffusion model with the assumption of the transparent interface [14, 15], the dependence of the spin signal on the distance  $d$  between the injector and the detector can be calculated as follows:

$$\Delta R_s \approx \frac{S_N}{S_{inj} S_{det}} \frac{P_F^2}{(1 - P_F^2)^2} \frac{\sigma_F^2 \lambda_F^2}{\rho_N \lambda_N \sinh(d/\lambda_N)}, \quad (1)$$

where  $\rho_F$  and  $\rho_N$  are the electrical resistivities for the Py and Cu, respectively.  $\lambda_F$  and  $\lambda_N$  are the spin diffusion length for Py and Cu, respectively.  $S_{inj}$ ,  $S_{det}$ , and  $S_N$  are the size of the injecting junction, the detecting junction, and the cross section of the

Cu wire, respectively.  $P_F$  is the spin polarization. From the fitting, one finds that the spin diffusion length for the Cu wire is 500 nm at RT and 1.5  $\mu\text{m}$  at 77 K.

In the nonmagnetic metals with weak spin orbit interactions such as Cu, Al, and Ag, the spin diffusion length is a few hundred nm at RT [8–10, 13, 16–18]. This means that one can manipulate the spin current in the Cu even in lateral configuration by using advanced nano-fabrication techniques. On the other hand, in some metals with a strong spin-orbit interaction and most of FMs, the spin diffusion length is known to be a few nm or a few 10 nm [19]. This implies that the manipulation of the spin current is difficult in such metals using the lateral configurations. However, as introduced later, by the combination between the lateral configurations and the unique transport properties of the spin current, one can effectively manipulate the spin current even in such metals.

### Advantage of Lateral Configuration

The conventional electrical spin injection is performed by injecting the spin-polarized current from a single FM injector into NM [7, 8, 10]. In such cases, the direction of the spin accumulation in the NM is fixed by the magnetization of the FM injector. When two or more FM injectors are utilized, one may have greater control of the spin current and spin accumulation. Taking the advantage of the flexible probe configuration in lateral geometry, one can easily expand the simple nonlocal spin-valve concept to a multiterminal device. This provides high tunability and the attractive device performance [10]. Here, two representative advantages using multiterminal spin injection are introduced.

The first demonstration is a direction control of the spin current using noncollinear dual spin injectors [20]. A lateral spin valve consisting of two Permalloy injectors Py1 and Py2 and a detector Py3, bridged by a Cu strip, has been prepared, as shown in a scanning electron microscope (SEM) image of Fig. 2. Here, the Py injectors are patterned into needle shapes so as to prevent the influence of the demagnetizing field in the remanent state. The easy axes of the Py injectors are tilted from the horizontal axis. The direction of the accumulated spin under the dual spin injection is detected by the Py strip with a horizontal easy axis as a nonlocal spin-valve signal.

The nonlocal spin-valve signal curves for various injected current fraction are shown in Fig. 3c. In the measurement, the magnetic field was swept between 600 and 400 Oe, to fix the magnetization direction of the detector Py3 during the sweep. In the nonlocal spin-valve signal under the dual injection shown in Fig. 3, the accumulated spin is not collinear with the detector, except when  $\phi = 0$  for  $i_2 = i_2$ , where  $\phi$  is the angle of the accumulated spin with respect to  $x$  axis. The spin signal  $\Delta R_s$  for noncollinear structures is defined as

$$\Delta R_s \equiv \frac{\Delta V(\phi)}{I_0(\phi)} = \frac{\Delta V(\phi)}{I_s(\phi)/p}, \quad (2)$$

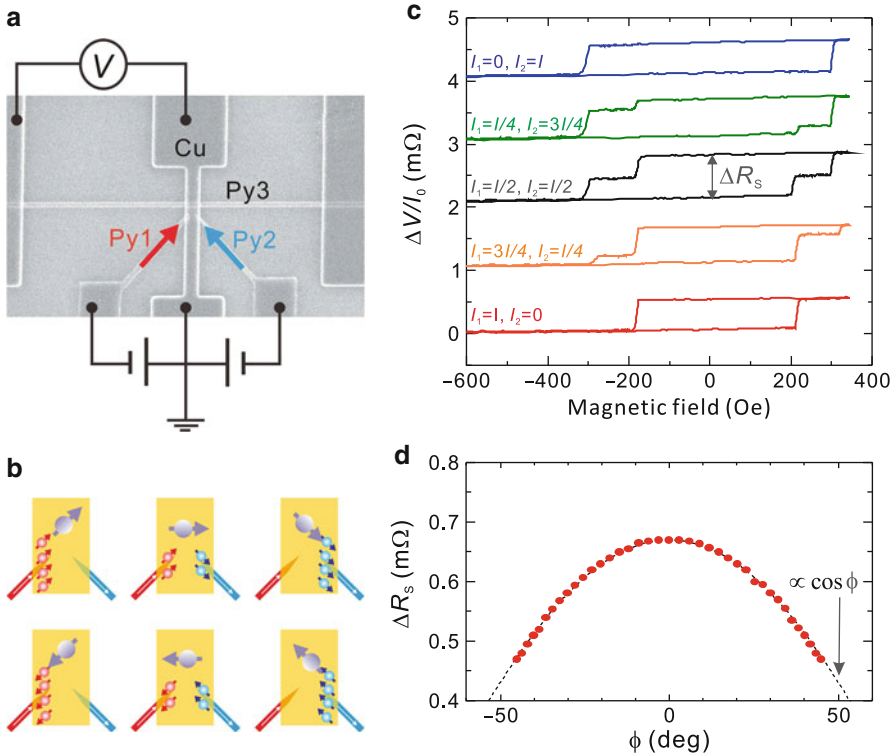


**Fig. 3** (a) SEM image of the lateral spin valve with the noncollinear dual spin injectors, (b) schematic illustration for electrical control of the direction of the spin accumulation using the noncollinear dual spin injectors, (c) nonlocal spin signal  $\Delta V/I_0$  for various current fraction, and (d) relationship between the direction of the accumulated spin and the spin signal

where  $I_s(\phi)$  is the magnitude of the spin current as a function of  $\phi$  and  $p$  is the spin polarization. As shown in Fig. 3d, under the condition that the charge current is held fixed as  $\phi$  is varied, one finds that  $\Delta R_s$  varies as  $\cos \phi$ . Thus, by injecting current through two magnetic wires with noncollinear configuration, it is possible to control electrically the polarization direction (axis) of the spin current. In this manner, one can rotate the polarization axis of the spin accumulation in the normal Cu wire while maintaining the magnetization direction of the spin detector fixed.

Then, the author focuses on the generation of the giant spin current using multiterminal spin injectors [21], which is the second advantage of the multiterminal injection. Since the conventional direct spin injection produces an extra Joule heating induced by the charge current, the magnitude of the injecting spin current is limited by the maximum tolerance of the charge current. On the other hand, the pure spin current does not include any charge current. Therefore, the maximum tolerance of the pure spin current is much larger than that of the spin-polarized current. This implies that one can inject giant spin currents, which cannot

be realized by the conventional direct spin injection. Moreover, pure spin current does not produce current-induced Oersted field. Thus, pure spin current is advantageous compared with the spin current induced by the conventional direct spin injection. Another example in this regard is that one may reverse the magnetization in the large dimension of the NM by the pure spin current injection [22–25]. Since the switching speed of the magnetization is proportional to the magnitude of the injecting spin current [26], the generation of the giant pure spin current may open the door for the ultrahigh-speed operation of the spintronic devices. The pure spin current is, in general, created by a nonlocal spin injection, and the magnitude is limited by the maximum allowed current in a ferromagnetic spin injector. If the pure spin current from two or more ferromagnetic injectors can be superimposed, one obtains a giant pure spin current, which is unachievable in the conventional spin injection. Therefore, here, a method for generating giant pure spin currents using multiterminal spin injection is introduced.

To demonstrate the multiterminal spin injection, a lateral spin valve consisting of the quadruple spin injectors (Py1, Py2, Py3, and Py4) has been fabricated. Figure 4a shows the scanning electron microscope image of the fabricated device together with its schematic. In order to create the spin current in Cu, the current  $I_C$  is injected from each injector. This means that totally  $4I_C$  current is provided from the current source. The spin signal can be evaluated by measuring the voltage between

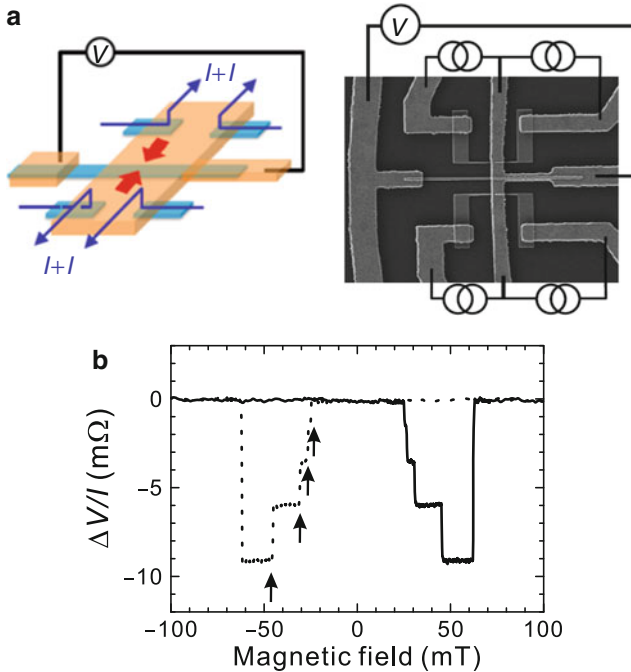


**Fig. 4** (a) Concept for multiterminal spin injection and SEM image of the multiterminal spin injection device. (b) Typical nonlocal spin-valve signal under quadruple spin injection

the middle Py and the Cu wire, as schematically shown in Fig. 4a. Figure 4b shows a typical nonlocal spin signal under the quadruple-terminal spin injection. The vertical axis corresponds to the value of the induced voltage divided by the injecting current  $I_C$  from each electrode. The signal shows large clear spin-valve effect consisting of four downward jumps and one upward jump. The four downward resistance jumps correspond to the magnetization switching of the four spin injectors. The spin current injecting into the middle Py wire is roughly estimated from the following equation [14, 22]:

$$I_S = \frac{1 - P_{Py}^2}{2P_{Py}} \frac{S_{det}}{\rho_{Py}\lambda_{Py}} \Delta R_S I_C. \tag{3}$$

This means that the injection spin current is proportional to the current in each terminal. Since the maximum tolerance current in the lateral spin-valve device is, in general, limited by the electromigration of the FM injectors, the maximum magnitude of the pure spin current is further increased by using thicker spin injectors.

One should also consider the influence of the heating under the high bias current injection because the heating of the sample strongly affects the spin transport. Therefore, the bias current dependence of the nonlocal spin-valve signal with varying number of the injectors has been investigated. In this experiment, the thickness of the Py injector was set to 25 nm, in order to heat the sample effectively. As shown in Fig. 5, if a single injector is used, at 1.5 mA, the spin signal reduces to 93 % of that at near-zero bias. On the other hand, for four-injector configuration, spin signal remains almost unattenuated at this injection level. This is due to the less heating of the Py injector for multiterminal case, compared to the single terminal case. It can be clearly confirmed that the critical current, where the spin signal starts to reduce, is improved by increasing the number of the spin injector. Thus, by using multiterminal spin injector, the Joule heating problem and electromigration issue in nonlocal spin injection can be tackled.

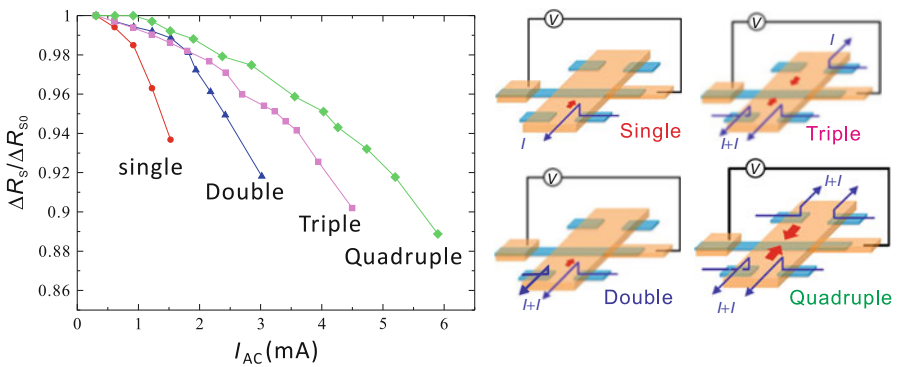


**Fig. 5** Bias dependence of the spin signals under single, dual, triple, and quadruple spin injections together with the schematics for each injection configuration

## Spin Absorption Effect

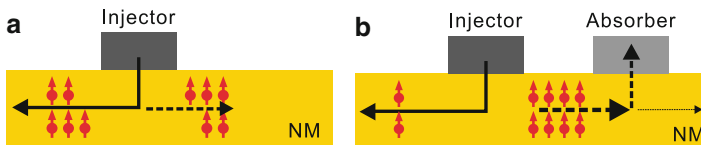
### Influence of an Additional Contact

The driving force of the pure spin current is a diffusion of the nonequilibrium electrons into the equilibrium state. If one considers the spin current in a single FM/NM junction shown in Fig. 6a, the spatial distribution of the spin accumulation in the NM symmetrically decays from the junction. Therefore, the spin current flows also symmetrically into both sides. On the other hand, when an additional material is connected in the right-hand side of the NM through the low resistive ohmic junction as in Fig. 6b, the spatial distribution of the spin accumulation is strongly modified. When the spin relaxation rate for the connected material is much larger than that for the NM, the nonequilibrium spins are preferably absorbed into the connected material. Thus, one can selectively extract the spin current. This is known as the spin absorption effect [15].

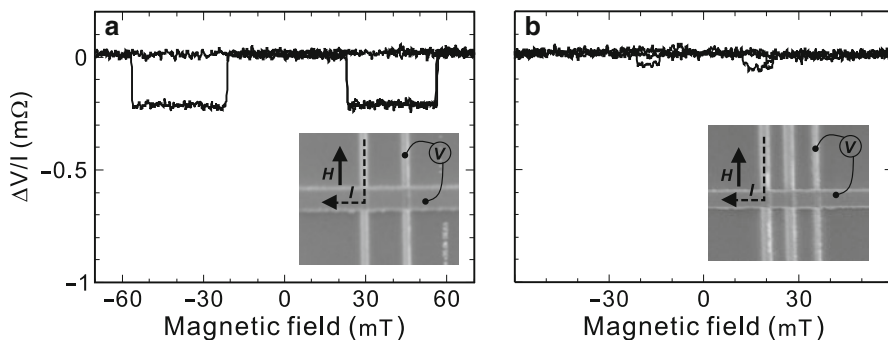
To demonstrate the above spin current absorption effect, two kinds of the lateral spin valves have been prepared [27]. One is a conventional lateral spin valve consisting of the Py injector and the detector bridged by a Cu strip (device A). The other one is a lateral spin valve with a middle Py wire (device B). Here, the center-center distance between the injector and the detector for device A is 600 nm, while that for device B is 460 nm. Although the geometrical disorder due to the additional ferromagnetic contact may also violate the spin coherence and the spin accumulation, such an effect should be negligible because of large difference in thickness between Cu and Py.

Figure 7a shows the spin signal observed in device A, where a spin-valve signal with the magnitude of 0.2 m $\Omega$  is clearly observed. Since the center-center distance between the injector and detector for device B is shorter than that for device A, one may naively expect that the larger spin signal is expected to be observed in device B. However, as in Fig. 7b, a quite small spin signal less than 0.05 m $\Omega$  is observed in device B. This is due to the influence of the spin current absorption into the middle Py wire and clearly support that the spin accumulation in the Cu is strongly suppressed by the middle Py2 wire connected to the Cu.

It was also demonstrated that the spin accumulation in the Cu is suppressed by connecting the nonmagnetic wire with a strong spin relaxation [15]. Figure 8 shows the spin signals with various nonmagnetic middle wires. Here, the center-center distance between the injector and detector is fixed at 600 nm. For the middle Cu



**Fig. 6** Schematic illustrations of the flow of the spin current in (a) single F/N junction and (b) an F/N junction with an F contact



**Fig. 7** (a) Nonlocal spin-valve signal for a conventional lateral spin valve and that for a lateral spin valve with a middle Py wire. The insets show SEM images of the measured device and the probe configurations for the nonlocal spin-valve measurements

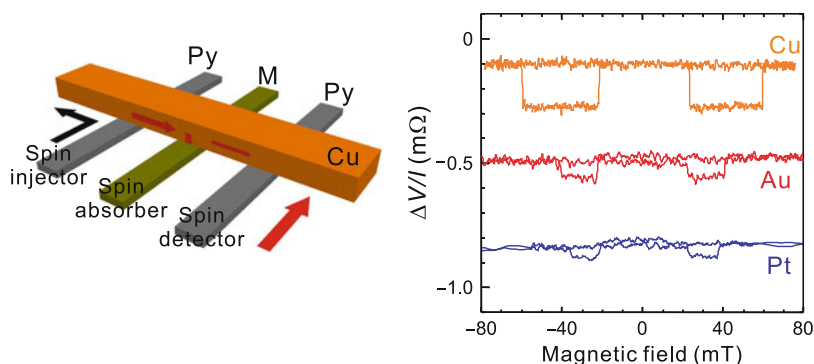


**Fig. 8** Nonlocal spin-valve signals for Cu, Au, and Pt middle wire measured at room temperature

wire, the obtained spin signal is 0.18 m $\Omega$ , which is almost the same as that without the middle wire. The large reductions of the spin signals are observed in the Au and Pt middle wires. These indicate that the nonequilibrium spin currents are strongly relaxed by the Pt and Au wires while the Cu has weak relaxation of the spin current. Thus, one can evaluate the magnitude of the spin relaxation of a material from the magnitude of the spin signal.

### Transverse Spin Current Absorption into Ferromagnetic Metal

Another interesting phenomenon is expected in the spin absorption into an FM. When the magnetization of the spin absorber is parallel or antiparallel to the injected spins (longitudinal spin absorption), the effective spin polarization is the same as that of the bulk spin polarization. This situation is known as a collinear configuration, which corresponds to most of the experimental situations in the

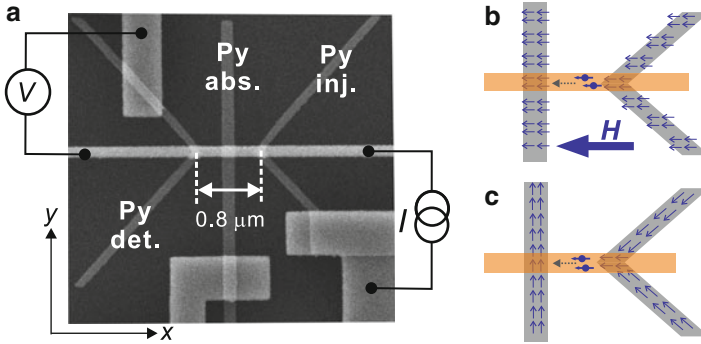


**Fig. 9** (a) Scanning electron microscope (SEM) image of the specially fabricated Py/Cu lateral spin valve consisting of two V-shaped nanowires with a middle strip. Expected domain structures in the Py wires and spin accumulation in a Cu channel for the longitudinal configuration (b) and the transverse configuration (c)

lateral spin-valve systems [8–11, 13, 17, 18]. On the other hand, when the magnetization of the spin absorber is normal to the direction of the spin current (transverse spin absorption), the effective spin polarization becomes zero [15]. Since the spin relaxation rate decreases with increasing the spin polarization, the spin relaxation rate for the transverse spin current becomes larger than that for the longitudinal spin current. Moreover, in the FM, the spin relaxation length for the transverse spin current is known to be shorter than that for the longitudinal one [28–32]. Since the spin relaxation rate is inversely proportional to the spin relaxation length, the shorter transverse spin relaxation length induces the further enhancement of the spin absorption into the middle Py wire. Therefore, one expects that the spin absorption can be tuned by the direction of the injected spin.

In order to evaluate the longitudinal and transverse spin current absorptions precisely, a lateral spin valve (LSV) using V-shaped ferromagnetic injector and detector shown in Fig. 9a has been fabricated [33]. Here, an FM strip, which plays a role of the spin absorber, is located in the middle of the V-shaped wires. The three ferromagnetic Py wires are bridged by a nonmagnetic Cu strip. It should be noted that the V-shaped Py wires are connecting with the Cu strip at the corners of the V-shaped wires. Therefore, the directions of the injecting and detecting spins reflect the domain structures at the corners. When the strong magnetic field is applied to the sample along the  $x$  direction, all of the magnetizations in the V-shaped wires and the strip are aligned with the  $x$  direction as shown in Fig. 9b. In this situation, the direction of the generated spins in the Cu strip is parallel to the magnetization of the spin absorber. This situation corresponds to the longitudinal spin current absorption. On the other hand, when the magnetic field decreases to zero, the domain structure of each FM wire reflects its own shape, as shown in Fig. 9c. The magnetization of the middle strip is aligned with the wire direction ( $y$  direction) because of the shape anisotropy. However, the magnetizations of the V-shaped wire around the corner maintain the field direction ( $x$  direction) even at the remanent

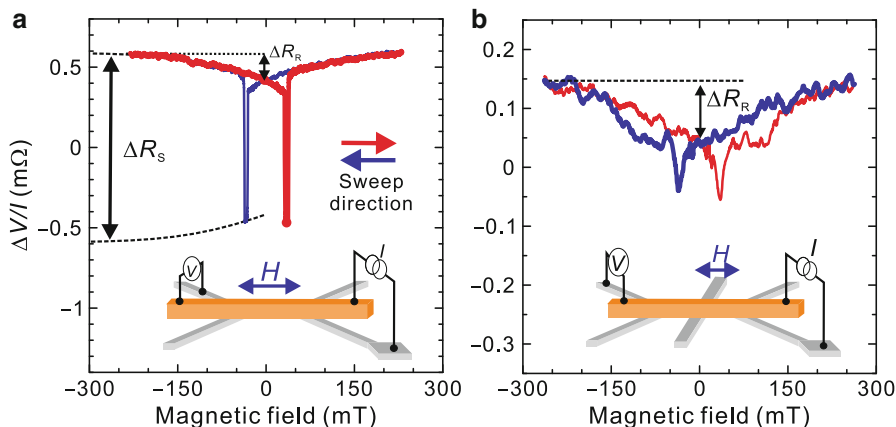


**Fig. 10** Nonlocal spin-valve signals for V-shaped LSV without a middle Py strip (a) and with a middle strip (b). Here, the magnetic field is applied along the x direction

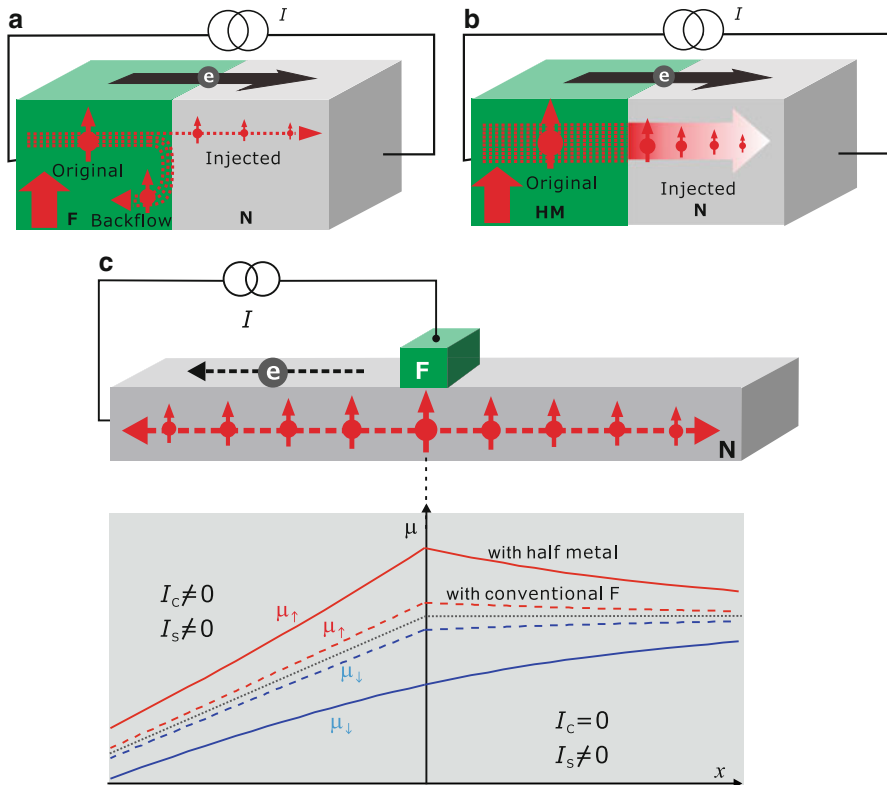
state [34]. In this situation, the injecting spin is perpendicular to the magnetization of the spin absorber, meaning the transverse spin current absorption. Note that the magnetic configuration between the injector and the detector should be roughly still in parallel at the remanent state. Therefore, the difference in the spin signal between two situations should be mainly caused by the change of the spin relaxation rate due to the middle Py wire. By comparing the nonlocal spin voltages between two situations, one can fairly evaluate the longitudinal and transverse spin current absorptions.

Figure 10a, b shows the nonlocal spin-valve signals for the V-shaped LSV with and without a middle ferromagnetic injector, respectively. The overall resistance change was estimated to be 0.3 mΩ, which is strongly reduced from the V-shaped LSV without the middle Py insertion (1.2 mΩ). This is due to the spin absorption effect into the middle Py strip [27]. More interestingly, in the LSV with the middle wire, the spin signal at the remanent state shows the significant reduction from the value at the high magnetic field. As mentioned above, the relative angle between the injecting spin and the magnetization direction of the middle wire becomes 90 at zero magnetic field. Therefore, the reduction of the spin signal in the low magnetic field is caused by the stronger spin absorption due to the transverse spin current. From the analysis based on one-dimensional spin diffusion model, the transverse spin relaxation length is 1.7 nm, which is much shorter than the longitudinal one (5 nm). Thus, it was experimentally demonstrated that the transverse spin current is absorbed by the FM more strongly than the longitudinal one.

## Reabsorption Effect of Spin Current

One should also take into account the spin absorption into the spin injector (reabsorption effect). By using the electrical spin injection, the nonequilibrium

spin accumulation is induced at the interface and diffused into the equilibrium state. In that case, the spin current diffuses not only into the NM but also into the FM injector. Notably, as mentioned above, the conventional ferromagnetic injector has much faster spin relaxation rate than that for the NM. Therefore, the injected spin current in the NM mainly returns back to the FM (Fig. 11a). This phenomenon gives rise to an extremely low injection efficiency of the spin current in the N [15, 35, 36]. However, if one utilizes a highly spin-polarized ferromagnet (HSF) as a spin injector, so-called half-metallic ferromagnet (HMF) [37], the spin-polarized electrons can be efficiently injected into the N, and the backflow of the spin currents can be strongly suppressed, resulting in a dramatic improvement of the injection efficiency of the spin currents in the N (Fig. 11b). This is because the spin relaxation rate for the FM is proportional to  $1 - P^2$ . In this scheme, the use of HSF spin injectors is critical for generating a giant pure spin current in the NM (Fig. 11c). Recently, significant improvement of the generation efficiency of the pure spin current has been achieved by using the spin injector consisting of the Heusler compound [38–40].



**Fig. 11** Schematic illustrations of the electrical spin injection from a conventional FM (a) and a HMF (b) into an NM. (c) Generation of a pure spin current by using nonlocal spin injection and spatial distributions of the spin-dependent electrochemical potentials in the N

The above-explained reabsorption effect can be characterized by the generation efficiency  $\eta$  given by the following equation [15]:

$$\eta = P \frac{\rho_F \lambda_F / (1 - P^2)}{\rho_N \lambda_N + \rho_F \lambda_F / (1 - P^2)}. \quad (4)$$

Here,  $\rho_N \lambda_N$  and  $\rho_F \lambda_F / (1 - P^2)$  correspond to the difficulty of the spin relaxations for the NM and FM, respectively. Therefore, the reabsorption effect can be understood as the competition of the spin relaxation strengths between FM and NM. Since the spin diffusion length for the ferromagnet  $\lambda_F$  is extremely short,  $\eta$  becomes very small in a conventional FM/NM junction. However, as explained above, by using a HMF with  $P \approx 1$ , the difficulty of the spin relaxation becomes very high. As a result,  $\eta$  is dramatically improved.

The difficulty of the electrical spin injection in an FM/semiconductor interface known as a conductance mismatch can be similarly understood by the spin reabsorption effect [36]. Since the electrical resistivity for the semiconductor is much larger than that for the FM,  $\eta$  becomes very small. A similar obstacle occurs in the case for the spin injection into the molecular materials because of their high resistivity. As explained above, a spin injector with a perfect HMF property can solve this issue. The spin injection efficiency is also known to be improved by inserting the tunnel barrier at the interface instead of the use of the highly spin-polarized material [41]. Since the insertion of the tunnel barrier strongly prevents the diffusion of the spin current into the FM injector, the difficulty of the spin relaxation for the FM is effectively enhanced. The preparation of a high-quality tunnel barrier without reducing the spin polarization at the interface is required for the effective spin injection. Since a long spin diffusion length is expected in silicon- and carbon-based organic materials, the efficient generation of the spin current in such materials may open a new avenue for the spintronic devices based on pure spin currents.

A contact size in the FM/NM junction is also an important factor for the spin injection, absorption, and reabsorption [42]. So far, the distance between the spin injector and detector is known as the most important geometrical parameter for the spin injection and detection. However, by reducing the size of the injecting junction, the generation efficiency of the pure spin current is drastically improved. This is because the spin relaxation rate in the FM is inversely proportional to the junction size  $S$ . To demonstrate this, the junction-size dependence of the spin signal has been investigated. Here, the junction size for the lateral spin valve is changed from  $0.006 \mu\text{m}^2$  to  $0.2 \mu\text{m}^2$  although the edge-to-edge distance between the injector and detector is fixed to 800 nm. Since the spin relaxation rate of the vertical Cu arms is small, the spin current diffusions into the horizontal Cu arms can be neglected. Then, the spin signal for the present LSV is roughly obtained by Eq. As mentioned above, reducing the size of the ohmic junction between the Py pad and the Cu wire decreases the spin relaxation rate in the Py pad. To change the junction size between the Py pad and the Cu wire, the length of the Cu wire on the Py pad is adjusted, as seen in the inset of Fig. 12c. The junction-size dependence of the spin signal has

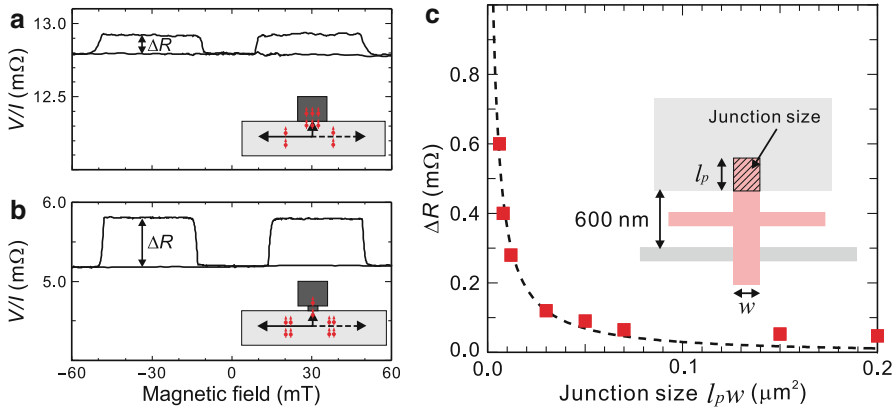


**Fig. 12** Nonlocal spin-valve signals of (a) the large-junction device and (b) the small-junction device with the probe configurations. (c) Spin signal in the NLSV measurement as a function of the junction size  $l_p w$ . The dotted curve is the best fitting to the data points using Eq. 4

been investigated by changing the size of the detecting junction with keeping the same electrode spacing of 600 nm. The obtained spin signal is plotted as a function of the junction size in Fig. 12c. The spin signal increases with reducing the junction size and is well reproduced by Eq. 1, where the spin signal is inversely proportional to the junction size.

## Magnetization Switching Due to Injection of Pure Spin Current

The switching mechanism due to spin torque is explained with a model proposed by Slonczewski in which the torque exerted on the magnetization is proportional to the injected spin current. This clearly indicates that the spin current is essential to realize the magnetization switching due to the spin injection. Most of the present spin-transfer devices consist of vertical multilayered nanopillars in which typically two magnetic layers are separated by a nonmagnetic metal layer [43, 44]. In such vertical structures, the charge current always flows together with the spin current; thereby, undesirable Joule heat is generated. As mentioned above, by optimizing the junction, the pure spin current can be effectively injected into the nanomagnet because of the spin absorption [42]. Therefore, the magnetization of nanomagnet can be switched nonlocally. To test this idea, a nanoscale ferromagnetic particle is configured for a lateral nonlocal spin injection device as in Fig. 13a, b [22–25].

The device for the present study consists of a large Permalloy (Py) pad 30 nm in thickness, a Cu cross 100 nm in width and 80 nm in thickness, and a Py nanoscale particle, 50 nm in width, 180 nm in length, and 6 nm in thickness. A gold wire 100 nm in width and 40 nm in thickness is connected to the Py particle to increase the effective spin relaxation rate, resulting in high spin current absorption into the Py particle. The magnetic field is applied along the easy axis of the Py particle.

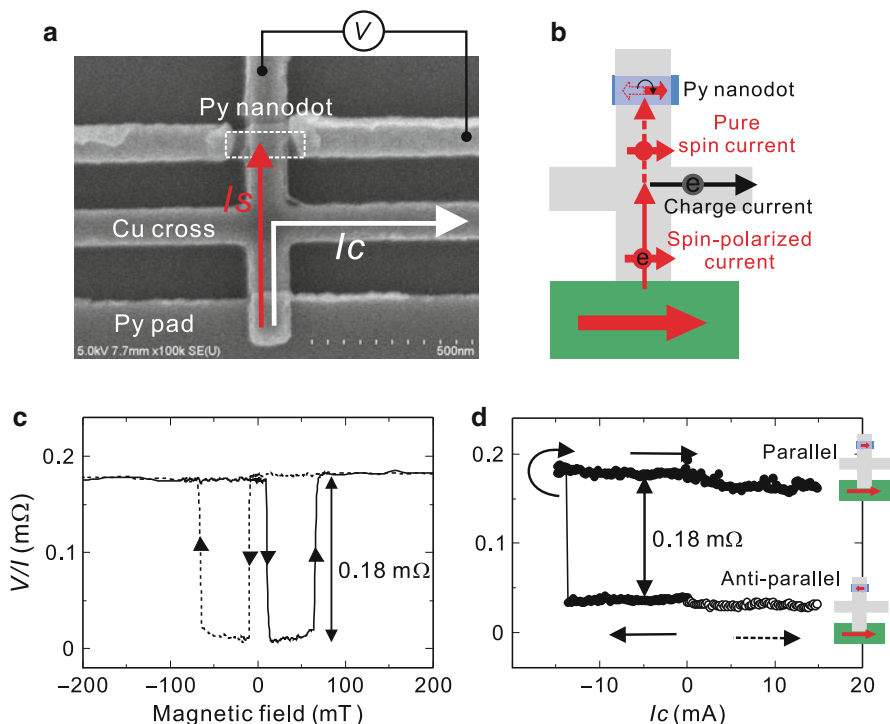


**Fig. 13** (a) Scanning electron microscope image of the fabricated lateral spin valve. (b) Schematic illustration of nonlocal spin injection using lateral spin-valve geometry. (c) Field dependence of the nonlocal spin signal. (d) Nonlocal spin-valve signal after the pulsed current injection as a function of the current amplitude with corresponding magnetization configurations

Here, the dimensions of Py pad and Cu wires are chosen large so that the charge current up to 15 mA can flow through them.

To confirm that the spin current from the Py injector is injected into the Py particle, the nonlocal spin-valve measurements are performed. As in Fig. 13c, the field dependence shows a clear spin signal with a magnitude of 0.18  $m\Omega$ , assuring that the spin current reaches the Py particle. Then, the effect of the nonlocal spin injection into the Py particle has been examined with using the same probe configuration. Before performing the nonlocal spin injection, the magnetization configuration is set in the antiparallel configuration by controlling the external magnetic field.

The nonlocal spin injection is performed by applying large pulsed currents up to 15 mA in the absence of magnetic field. As shown in Fig. 13d, when the magnitude of the pulsed current is increased positively in the antiparallel state, no signal change is observed up to 15 mA. On the other hand, for the negative scan, the abrupt signal change is observed at  $-14$  mA. The change in resistance at  $-14$  mA is 0.18  $m\Omega$ , corresponding to that of the transition from antiparallel to parallel states. This means that the magnetization of the Py particle is switched only by the spin

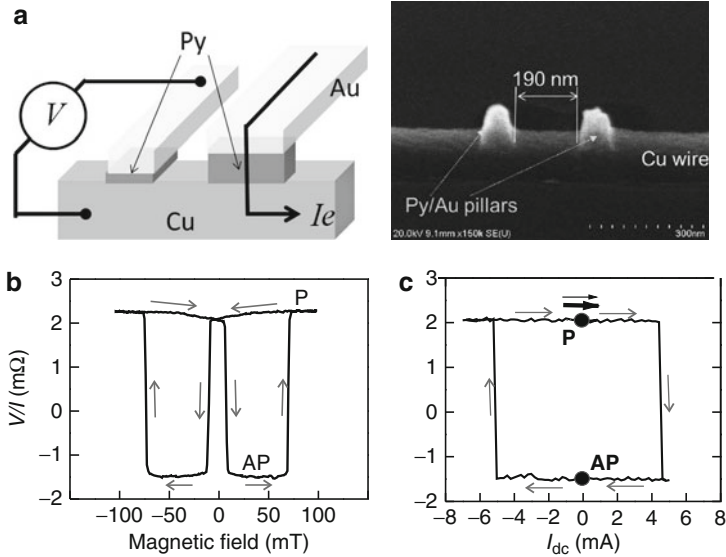


**Fig. 14** (a) SEM image and schematic illustration of the improved nonlocal spin injection device. (b) Giant spin signal and (c) the reversible magnetization switching by the pure spin current injection observed in the improved device

current induced by the nonlocal spin injection. The responsible spin current for switching is estimated from the experiment to be about 200  $\mu\text{A}$ , which is reasonable compared with the values obtained for conventional pillar structures. However, the switching from the parallel to antiparallel state has not been achieved in the present device. This is mainly due to the low spin-injection efficiency.

To improve the efficiency of the injecting spin current, a newly designed sample has been fabricated, as shown in Fig. 14a [23]. The new sample consists of two Py/Au nanopillars on a Cu wire. As shown in Fig. 14a, the junction size between the Py and Cu in the new sample is effectively diminished, leading to the efficient generation of the pure spin current. Figure 14b shows the nonlocal spin-valve signal as a function of the external field. The obtained spin signal is around 4 m $\Omega$ , much larger than that of the previous device. Then, nonlocal spin injection with variable DC current is applied to perform the magnetization switching. The sample is preset to a parallel state at which both magnetizations are aligned in the positive field direction. As can be seen in Fig. 14c, when the current is increased, the nonlocal spin-valve signal sharply decreases at about 4.5 mA, indicating a clear magnetization reversal. According to the change in the nonlocal spin-valve signal, the parallel state is transformed into an antiparallel state which is switched back to the parallel state by a negative DC current of 5 mA. Thus, reversible magnetization switching between antiparallel and parallel states is realized by means of nonlocal spin injection with the specially developed device consisting of perpendicular nanopillars and lateral magnetic nanostructures.

Very recently, Zou and Ji demonstrate the nonlocal switching of the Py nanodot by using a specially developed LSV structure [24]. They prepared a lateral spin valve with a 5-nm-thick ferromagnetic Py detector. This structure enables to inject the pure spin current entirely in the Py detector. As a result, the magnetization of the Py detector is reversed by a sufficiently large spin torque. The interesting thing is that the structure includes the interface barriers both at the injecting and detecting junctions. According to the spin diffusion model, the interface resistance strongly suppresses the spin current diffusion into the ferromagnet. To understand the result more quantitatively, other effects such as the magnetic interface anisotropy may have to be considered.

---

## Conclusion and Outlook

The author described the transport properties of the diffusive spin currents by introducing the experimental studies on the electrical spin injection in metallic nanostructures. The author shows that a nonlocal spin injection in a lateral spin-valve structure enables to create a pure spin current. Electrical control of the direction of the spin accumulation and the generation of the giant pure spin current were demonstrated by the multiterminal spin injections. The author also shows that the diffusion process of the spin current is strongly affected by the spin absorption and reabsorption effects. The magnetization switching of the ferromagnetic nanodot due to the pure spin current injection was demonstrated.

A novel manipulation and sensitive detection techniques of the pure spin currents have been developed recently by using the spin Hall effect [45–47]. Moreover, the spin current is found to be generated from the heat flow [48] and to transport even in electrical insulator [49]. These novel techniques may open up possibilities for new spintronic devices with ultralow power consumptions. However, the application feasibility of the pure spin currents is still low at moment because of the low generation efficiency of the pure spin current. Further improvements should be achieved for the practical application of the pure spin current. Very recently, a room-temperature magnetization switching using the pure spin current induced by the spin Hall effect has been demonstrated [50]. This innovative demonstration may revolutionize the realization of more functional spin devices utilizing pure spin currents.

**Acknowledgment** The author would like to thank Prof. Otani for the valuable discussions and the financial supports from NEDO and CREST.

---

## References

1. Wolf SA et al (2001) Spintronics: A Spin-Based Electronics Vision for the Future. *Science* 294:1488
2. Zutic I, Fabian I, Das Sarma S (2004) Spintronics: Fundamentals and applications. *Rev Mod Phys* 76:323
3. Chappert C, Fert A, Van Dau Nguyen F (2007) The emergence of spin electronics in data storage. *Nat Mater* 6:813–823

4. Maekawa S, Valenzuela SOV, Saitoh E, Kimura T (eds) Spin current. Oxford University Press
5. Pratt WP Jr, Lee S-F, Slaughter JM, Loloee R, Schroeder PA, Bass J (1991) Perpendicular Giant Magnetoresistances of Ag/Co Multilayers. *Phys Rev Lett* 66:3060
6. Brataas A, Kent AD, Ohno H (2012) Current-induced torques in magnetic materials. *Nature Mater*. *Nat Mater* 11:372–381
7. Johnson M, Silsbee RH (1987) Thermodynamic analysis of interfacial transport and of the thermomagneto-electric system. *Phys Rev B* 35:4959
8. Jedema FJ, Filip AT, van Wees BJ (2001) Electrical spin injection and accumulation at room temperature in an all-metal mesoscopic spin valve. *Nature (London)* 410:345
9. Valenzuela SO (2009) Nonlocal Electronic Spin Detection, Spin Accumulation and the Spin Hall effect. *Int J Mod Phys B* 23:2413
10. Kimura T, Otani Y (2007) Spin transport in lateral ferromagnetic/nonmagnetic hybrid structures. *J Phys J Phys Cond Mat* 19:165216; Otani Y, Kimura T (2011) Spin current related phenomena in metallic nano-structures. *Physica E* 43:735
11. Hoffmann A (2007) Pure Spin-Currents. *Phys Stat Sol (c)* 4:4236
12. Bader SD, Parkin SSP (2010) Spintronics. *Annu Rev Condens Matter Phys* 1:71
13. Urech M, Korenivski V, Poli N, Haviland DB (2006) Direct Demonstration of Decoupling of Spin and Charge Currents in Nanostructures. *Nano Lett* 6:871
14. Takahashi S, Maekawa S (2003) Spin injection and detection in magnetic nanostructures. *Phys Rev B* 67:052409
15. Kimura T, Hamrle J, Otani Y (2005) Estimation of spin-diffusion length from the magnitude of spin-current absorption: Multiterminal ferromagnetic/nonferromagnetic hybrid structures. *Phys Rev B* 72:014461
16. Mihajlovic G et al (2010) Enhanced spin signals due to native oxide formation in Ni<sub>80</sub>Fe<sub>20</sub>/Ag lateral spin valves. *Appl Phys Lett* 97:112502
17. Garzon S, Zutic I, Webb RA (2005) Temperature-Dependent Asymmetry of the Nonlocal Spin-Injection Resistance: Evidence for Spin Nonconserving Interface Scattering. *Phys Rev Lett* 94:176601
18. van Staa A, Wulffhorst J, Vogel A, Merkt U, Meier G (2008) Spin precession in lateral all-metal spin valves: Experimental observation and theoretical description. *Phys Rev B* 77:214416
19. Bass J, Pratt WP Jr (2007) Spin-diffusion lengths in metals and alloys, and spin-flipping at metal/metal interfaces: an experimentalist's critical review. *J Phys Condens Matter* 19:183201
20. Kimura T, Otani YC, Levy PM (2007) Electrical Control of the Direction of Spin Accumulation. *Rev Lett* 99:166601
21. Nonoguchi S, Nomura T, Kimura T (2012) Electrical manipulation of spin polarization and generation of giant spin current using multi terminal spin injectors. *J Appl Phys* 111:07C505
22. Kimura T, Otani Y, Hamrle J (2006) Switching Magnetization of a Nanoscale Ferromagnetic Particle Using Nonlocal Spin Injection. *Phys Rev Lett* 96:037201
23. Yang T, Kimura T, Otani Y (2008) Giant spin-accumulation signal and pure spin-current-induced reversible magnetization switching. *Nat Phys* 4:851 4
24. Zou H, Ji Y (2011) Temperature evolution of spin-transfer switching in nonlocal spin valves with dipolar coupling. *J Magn Magn Mater* 323:2448; Zou H, Chen S, Ji Y (2012) Reversal and excitations of a nanoscale magnetic domain by sustained pure spin currents. *Appl Phys Lett* 100:012404
25. Sun JZ et al (2009) Publisher's Note: A three-terminal spin-torque-driven magnetic switch. *Appl Phys Lett* 95:083506
26. Sun JZ (2000) Spin-current interaction with a monodomain magnetic body: A model study. *Phys Rev B* 62:570–578
27. Kimura T, Hamrle J, Otani Y, Tsukagoshi K, Aoyagi Y (2004) Spin-dependent boundary resistance in the lateral spin valve structure. *Phys Lett* 85:3501
28. Zhang S, Levy PM, Fert A (2002) Mechanisms of Spin-Polarized Current-Driven Magnetization Switching. *Phys Rev Lett* 88:236601
29. Stiles MD, Zangwill A (2002) Anatomy of spin-transfer torque. *Phys Rev B* 66:014407

30. Zhang J, Levy PM, Zhang S, Antropov V (2004) Identification of Transverse Spin Currents in Noncollinear Magnetic Structures. *Phys Rev Lett* 93:256602
31. Taniguchi T, Yakata S, Imamura H, Ando Y (2008) Penetration depth of transverse spin current in ferromagnetic metals. *IEEE Trans Magn* 44:2636
32. Taniguchi T, Yakata S, Imamura H, Ando Y (2008) Determination of Penetration Depth of Transverse Spin Current in Ferromagnetic Metals by Spin Pumping. *Appl Phys Exp* 1:031301-1-3
33. Nonoguchi S, Nomura T, Kimura T (2010) Longitudinal and transverse spin current absorptions in a lateral spin-valve structure. *Phys Rev B* 86:104417
34. Taniyama T, Nakatani I, Namikawa T, Yamazaki Y (1999) Resistivity due to Domain Walls in Co Zigzag Wires. *Phys Rev Lett* 82:2780
35. van Son CP, van Kempen H, Wyder P (1987) Boundary resistance of the ferromagnetic-nonferromagnetic metal interface. *Phys Rev Lett* 58:2271–2273
36. Schmidt G, Ferrand D, Molenkamp WL, Filip TA, van Wees JB (2000) Fundamental obstacle for electrical spin injection from a ferromagnetic metal into a diffusive semiconductor. *Phys Rev B* 62:R4790–R4793
37. Balke B, Wurmehl S, Fecher HG, Felser C, Kubler J (2008) Rational design of new materials for spintronics:  $\text{Co}_2\text{FeZ}$  ( $Z = \text{Al, Ga, Si, Ge}$ ). *Sci Technol Adv Mater* 9:014102
38. Kimura T, Hashimoto N, Yamada S, Miyao M, Hamaya K (2012) Room-temperature generation of giant pure spin currents using  $\text{Co}_2\text{FeSi}$  spin injectors. *NPG Asia Mater* 4:e9. doi:10.1038/am.2012.16. <http://www.nature.com/am/journal/v4/n3/full/am201216a.html>
39. Bridoux G, Costache MV, Van de Vondel J, Neumann I, Valenzuela SO (2011) Enhanced spin signal in nonlocal devices based on a ferromagnetic  $\text{CoFeAl}$  alloy. *Appl Phys Lett* 99:102107
40. Takahashi YK, Kasai S, Hirayama S, Mitani S, Hono K (2012) All-metallic lateral spin valves using  $\text{Co}_2\text{Fe}(\text{Ge}_{0.5}\text{Ga}_{0.5})$  Heusler alloy with a large spin signal. *Appl Phys Lett* 100:052405
41. Rashba EI (2000) Theory of electrical spin injection: Tunnel contacts as a solution of the conductivity mismatch problem. *Phys Rev B* 62, R16267
42. Kimura T, Otani Y, Hamrle Phys J (2006) Enhancement of spin accumulation in a nonmagnetic layer by reducing junction size. *Rev B* 73:132405
43. Tsoi M, Jansen AGM, Bass J, Chiang W-C, Seck M, Tsoi V, Wyder Phys P (1998) Excitation of a Magnetic Multilayer by an Electric Current. *Rev Lett* 80:4281
44. Albert FJ, Emley NC, Myers EB, Ralph DC, Buhrman Phys RA (2002) Quantitative Study of Magnetization Reversal by Spin-Polarized Current in Magnetic Multilayer Nanopillars. *Rev Lett* 89:226802
45. Saitoh E, Ueda M, Miyajima H, Tataru G (2006) Conversion of spin current into charge current at room temperature: Inverse spin-Hall effect. *Appl Phys Lett* 88:182509
46. Valenzuela SO, Tinkham M (2006) Direct electronic measurement of the spin Hall effect. *Nature (London)* 442:176
47. Kimura T, Otani Y, Sato T, Takahashi S, Maekawa S (2007) Room-Temperature Reversible Spin Hall Effect. *Phys Rev Lett* 98:156601
48. Slachter A, Bakker FL, Adam JP, van Wees BJ (2010) Thermally driven spin injection from a ferromagnet into a non-magnetic metal. *Nat Phys* 6:879
49. Kajiwara Y, Harii K, Takahashi S, Ohe J, Uchida K, Mizuguchi M, Umezawa H, Kawai H, Ando K, Takanashi K, Maekawa S, Saitoh E (2010) Transmission of electrical signals by spin-wave interconversion in a magnetic insulator. *Nature (London)* 464:262
50. Liu L, Pai C-F, Li Y, Tseng H-W, Ralph DC, Buhrman RA (2012) Spin torque switching with the giant spin Hall effect of tantalum. *Science* 336:555